PERGAMON

Vacuum 65 (2002) 415–425

VACUUM
SURFACE ENGINEERING, SURFACE INSTRUMENTATION & VACUUM TECHNOLOGY

www.elsevier.com/locate/vacuum

Plasma spraying of micro-composite thermal barrier coatings

S. Sharafat[a], A. Kobayashi[b,*], Y. Chen[a], N.M. Ghoniem[a]

[a] *Mechanical and Aerospace Engineering Department, University of California Los Angeles, Los Angeles, CA 90095, USA*
[b] *Joining and Welding Research Institute, Osaka University, 11-1 Mihogaoka, Ibaraki, Osaka 567-0047, Japan*

Abstract

The thermal barrier coatings (TBCs) by gas tunnel-type plasma spraying exhibited ceramic-composite features consisting of a host oxide matrix ceramic with an embedded second phase material. The densities of the composite TBC were found to be higher than those sprayed with 100 wt% ZrO_2 or Al_2O_3. In the coatings produced with powder mixtures of 50 wt%, the embedded splats are found to have a relatively uniform thickness between 1 and 10 μm and they exhibited clear and pore-free interfaces with the host material. The micro-composite coatings also exhibited thickness-dependent functionally gradient Vickers hardness values by the hardness measurements across the coating thickness. A one-dimensional series heat transfer model was developed to estimate upper and lower bounds of the transverse thermal resistance as a function of alumina–zirconia weight ratio. The model shows that the addition of higher thermally conducting Al_2O_3 can result in an increase in the transverse thermal resistivity of YSZ.

Keywords: Plasma spraying; Gas tunnel-type; Thermal barrier-composite coatings; Aluminum oxide; Zirconium oxide; Vickers hardness; Resistivity

1. Introduction

Partially stabilized zirconia (PSZ) coatings are widely used in the aerospace and in the automotive industries [1–4]. As thermal barrier coatings (TBC), they not only reduce the substrate-metal temperature, but also protect the base against hot corrosion, oxidation, and wear damage. In the aerospace industry, the TBCs are used primarily to protect austenitic superalloy blades and vanes of gas turbine engines, turbine shrouds and combustor cans. These coatings increase the lifetime of components by increasing the turbine blade cooling efficiency, and in conjunction with MCrAlY bond-coats, prevent hot corrosion of the superalloy by molten salts and corrosive gases [5]. The automotive industry uses these coatings to protect components such as pistons, valves, and intake and exhaust ports against wear and corrosion particularly in diesel engines [5]. To increase fuel efficiency and to reduce levels of hydrocarbons in exhaust gases, the combustion temperatures need to be raised further. Development of thick TBC (up to 3 mm) with improved mechanical properties is critical to operation at a higher combustion temperature [6].

However, with increasing thickness, TBC exhibits higher residual stresses and a drop in adhesion strength. The development of micro-

*Corresponding author. Tel.: +81-6-6879-8694; fax: +81-6-6879-8689.
E-mail address: kobayasi@jwri.osaka-u.ac.jp (A. Kobayashi).

0042-207X/02/$ - see front matter
PII: S0042-207X(01)00451-1

composite TBC with improved mechanical properties, such as Young's modulus, shear modulus, hardness, and fracture strength is being pursued [6]. Modifications in the microstructure of coatings using graded porosity have met with limited success in reducing residual stress [7].

Another area of active research to improve TBC, particularly, reduction of oxygen diffusion, has been the development of composite coatings [8–10]. Using plasma spraying and electron-beam physical-vapor deposited (EB-PVD), alternating layers of ZrO_2 and Al_2O_3 are deposited. The development of an oxygen diffusion barrier into the TBC, which reduces the thermally grown oxide layer at the bond-coat/zirconia interface, is critical for improving turbine blade performance. An et al. [8] reported the thermal conductivity of alternating EB-PVD Al_2O_3 and Y_2O_3 stabilized zirconia layers. The total coating thickness was maintained at 100 μm. The thermal conductivity measurements showed no apparent effects of interface thermal resistance, because no significant decrease in thermal conductivity was observed for the higher number-layered coatings. It was reasoned that because layer growth occurs by epitaxy the development of discontinuities between the layers is reduced [8].

In contrast with EB-PVD-produced alternating alumina/zirconia layers, plasma-sprayed-laminated composites showed an increase in thermal resistance. Ramaswamy et al. measured the temperature drop and thermal shock resistance of coatings consisting of 2–3 alternating layers of 100–150 μm thick alumina and YSZ [9]. The double-layered alternating coatings showed a 20% increase in temperature drop compared with single-layered YSZ coatings. The thermal shock resistance of the laminated coatings was also found to be far superior to that of single bulk coatings.

Ravichandran et al. investigated the temperature dependence of the thermal conductivity of plasma-spray-deposited monolithic coatings, as well as multi-layer coatings that consisted of Al_2O_3 and 8YPS [10]. The laminated coatings exhibited a large reduction in the thermal conductivity at all temperatures when compared to the bulk monolithic. However, the multi-layer coatings showed little variation in the thermal conductivity, relative to the number of layers, which suggests that the influence of interlayer interfaces on heat transfer is relatively small. These results indicate good bonding between the Al_2O_3 and YSZ layers.

However, significant residual stresses can arise in alternating ceramic laminates during densification and cooling, which result in linear cavitation damage and curling behavior [11]. Thermal expansion mismatch stresses, which arise during cooling, can place the zirconia layers in residual biaxial tension and lead to the formation of transverse cracks. Green et al. [11] found that the addition of alumina to the zirconia layers was effective in reducing the sources of residual stresses and reduced the formation of cracks.

In this work, the development of a YSZ–Al_2O_3 ceramic composite coating by plasma spraying with mixtures of the powder was investigated. The purpose of this research is to develop thick TBC with improved mechanical and chemical properties without compromising the thermal properties of TBC. The advantage of such a TBC is that the alumina layer acts as an oxygen diffusion barrier and the sharp mismatches between thermal expansion coefficients of alumina and YSZ are eliminated. Such micro-composite TBCs by gas tunnel-type plasma spraying, with mixing ratios of YSZ to alumina (Al_2O_3) between 20 and 80 wt% were reported here. A simple one-dimensional (1-d) heat transfer model was developed to calculate the range of thermal resistance of the micro-composite coatings.

2. Experimental procedures

Fig. 1 shows the schematic of the gas tunnel-type plasma-spraying system. It consists of an axially fed hollow-cathode DC-plasma-gun and a vortex-stabilized plasma torch. The setup is described in detail elsewhere [12]. Operating conditions for deposition of the micro-composite TBC are presented in Table 1.

An 8 wt% Yttria-stabilized ZrO_2 (PSZ) powder and alumina powder were used. Particle size and chemical composition of the PSZ and the alumina

powders are given in Table 2. Three mixtures of ZrO_2/Al_2O_3 powders with wt% ratios of 80/20, 50/50, and 20/80 were used. The powder was fed using a powder feeder, which is based on the fluidized bed concept, without any moving parts. Spraying duration was kept below 30 s in order to maintain the powder feed rate constant.

The nozzle-substrate distance was varied between 50 and 60 mm. The substrate coupons were 50 mm25 mm3 mm SUS-304 stainless steel, which were grid-blasted and then chemically cleaned. No bond coat was used. Details of the spraying conditions are given in Table 3.

The edge-enhanced view elucidates the splat geometry. Therefore, the Scion-Image software was used for the image enhancement [13] in order to have a clear delineation between the two phases.

The Vickers Hardness (H_v) of the coatings was measured as a function of powder composition, spraying distance, and across the coating thickness as a function of distance from the free-coating surface.

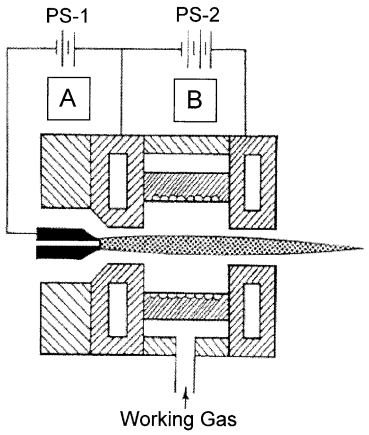

Fig. 1. Schematic diagram of gas tunnel-type plasma-spraying system. (A) axially fed hollow-cathode plasma gun, (B) vortex-stabilized plasma torch (PS-1 and PS-2 are power supplies for A and B, respectively).

3. Results

3.1. Micrographs

Fig. 2(a)–(c) depicts micrographs of coatings, respectively. Fig. 2(a) and (b) were produced using the hollow-cathode plasma gun at a low power of 6.5 kW. The spraying distance and spraying duration for both powder mixtures was 50 mm and 10 s, respectively. The micrograph in Fig. 2(a) was produced with an 80/20 wt% ratio of ZrO_2/Al_2O_3 powder. This shows a non-uniform distribution of highly, irregularly shaped zirconia (light gray) and alumina (dark gray) splats. The boundaries between the zirconia and the alumina splats are clearly discernable and relatively free of voids. For the 80/20 wt% powder mixture, the ratio of the cross-sectional area of the zirconia to that of alumina reflects that of the ratio of the powder mixture itself. Several few-μm diameter voids are present along the substrate-coating interface and concentrations of larger voids (10–20 μm) can be seen trapped close to the substrate.

The micrograph of Fig. 2(b) shows a coating made with a 50/50 wt% ZrO_2/Al_2O_3 powder

Table 1
Plasma-spray operating conditions

	Units	Hollow-cathode	Vortex-generator
Power	kW	5.3–6.5	12.5–21.5
Voltage (unloaded/load)	V	75/40	135/85
Working gas flow rate (Ar)	l/min	50–60	100–120
Carrier gas flow rate (Ar)	l/min	7	10–15
Powder feed rate	g/min	20–25	10–30
Spraying duration	s	10–30	5–15
Spraying distance	mm	40–60	40–70

Table 2
Properties of zirconia and alumina powders

Powder	Chemical composition (wt%)					Size (μm)
	ZrO_2	Y_2O_3	Al_2O_3	SiO_2	Others	
Zirconia	90.78	8.15	0.38	0.20	0.49	10–44
Alumina	98.5	—	—	1.0	0.5	15–53

Table 3
Operating conditions for coatings depicted in Fig. 2

Powder ZrO_2/Al_2O_3 (wt%)	80/20	50/50	50/50
Fig. 2	(a)	(b)	(c)
Plasma torch system	Plasma gun	Plasma gun	Gas tunnel-type
Power (kW)	6.5	6.5	21.5
Spraying distance (mm)	50	50	70
Spraying duration (s)	10	10	5
Working gas flow rate (l/min)	50	50	120
Powder feed rate (g/min)	22.7	20	12
Maximum thickness (μm)	450	500	420

mixture and with the same spraying conditions as those used to produce the coatings shown in Fig. 2(a). The ratio of cross-section area between zirconia and alumina is close to that of the premixed powder. However, the microstructure differs significantly between the 50/50 wt% and the 80/20 wt% coating. For the 50 wt% premixed powder the following observations were made:

(1) Both, the zirconia and the alumina splats exhibit "regular" geometry, consisting of fairly uniform splats of about 1–5 μm thick ZrO_2 embedded in an Al_2O_3 matrix. The majority of splats are oriented parallel to the substrate.
(2) Most of the voids are several μm in diameter and are distributed relatively uniformly throughout the coating. A relatively large concentration of voids is concentrated parallel to the substrate close to the coating surface.

Fig. 2 also compares the "edge-enhanced" image [13] of the 50 wt% and the 80/20 wt% ZrO_2/Al_2O_3 powder-based coatings. The edge-enhanced view elucidates the splat geometry and shows the change from irregularly shaped splats into elongated (flat) splats with increasing alumina. The orientation of the splats as a function of powder mixture ratio is apparent from the edge-enhanced views depicted in Fig. 2.

The interfaces between Al_2O_3 and ZrO_2 splats are sharp. Alumina and zirconia are insoluble into each other and the phase diagram shows the lack of formation of new phases [14]. The alumina/zirconia splat interfaces can, therefore, be considered to have sharp delineation between the two materials.

Fig. 2(c) shows the cross section of a coating deposited at high power (21.5 kW) using the vortex-stabilized plasma. The morphology of the coating is very similar to the low-power-plasma coating, which was also made with 50 wt% premixed powders. However, compared with the low-power-produced coatings there is a large difference in the ratio of the phases. The image analysis of the coatings reveals a ceramic composite with a constituent ratio ZrO_2/Al_2O_3 of 0.47 for the high-power-produced coatings and a value close to unity for the low-power-produced coatings.

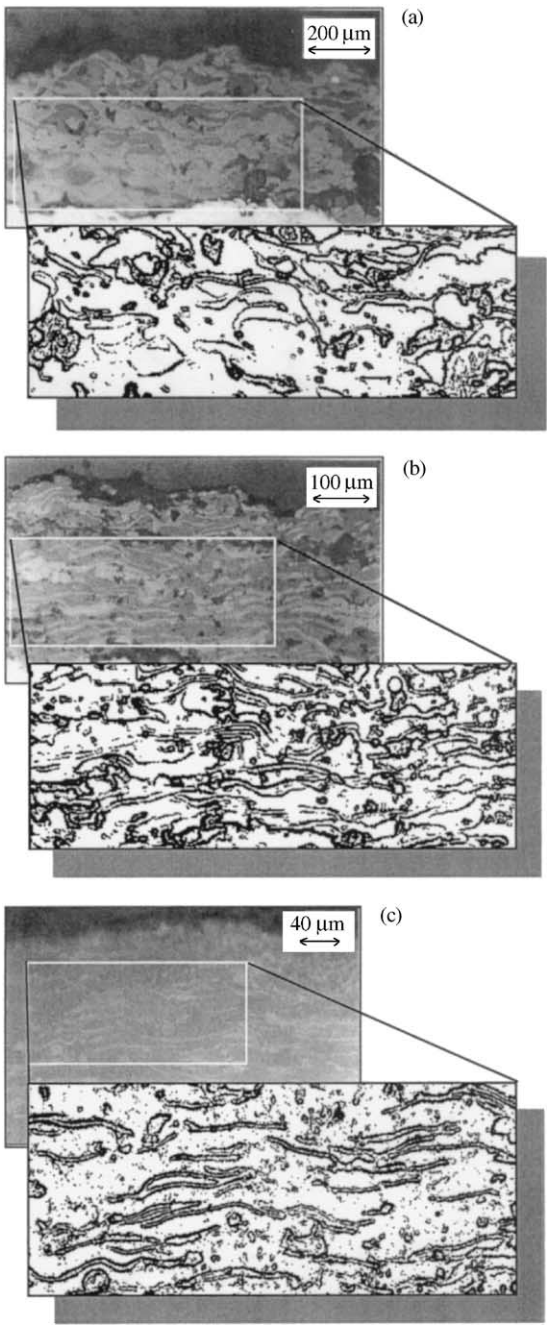

Fig. 2. Comparison of micrograph and the splat morphology of the micro-composite coatings. (a) 80/20 wt% ZrO_2/Al_2O_3 powder mixture, (b) 50/50 wt% ZrO_2/Al_2O_3 powder mixtures. (c) 50/50 wt% ZrO_2/Al_2O_3 powder mixture. (a) and (b) were produced using the hollow-cathode plasma-gun at low-power operation, and (c) was produced using the gas tunnel-type plasma torch at a power of 21.5 kW.

The excess zirconia indicates that the fraction of molten ZrO_2 reaching the substrates is a factor of two larger than Al_2O_3. High-power operation results in a disproportionately higher dissociation of Al_2O_3 compared with ZrO_2, because of the higher melting and boiling temperature of ZrO_2. Fig. 2(c) shows the "edge-enhanced" view of the high-power produced micro-composite. A comparison between the edge-enhanced view of Fig. 2(b) and (c) shows that the splat geometry is not very different even though the two coatings were produced at different power levels.

3.2. Hardness

Regarding the effect of powder composition on Vickers Hardness H_v, the H_v of the composite coatings were increased as the powder mixtures containing alumina were increased. For the powder mixtures above 70 wt% alumina, the H_v was approaching that of pure alumina.

The hardness of a 50/50 and a 70/30 wt% Al_2O_3/ZrO_2 powder mixture was measured as a function of spraying distance and the results are shown in Fig. 3. A premixed powder containing 70 wt% alumina results in a harder coating compared to 50 wt%. An increase in spraying distance results in

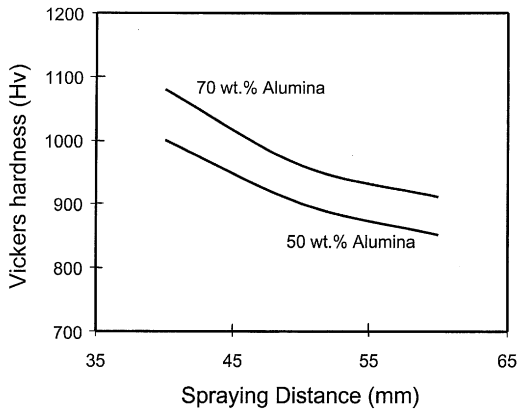

Fig. 3. Vickers hardness of two zirconia–alumina powder mixture-based coatings as a function of spraying distance (coatings produced with high-power gas tunnel-type plasma spraying for operating conditions in Table 3).

a decrease in the overall coating hardness for both powder ratios with similar trends.

Fig. 4 shows the hardness distributions across the coating thickness for the 50 and 80/20 wt% ZrO_2/Al_2O_3-produced coatings. The hardness of the 50 wt% coating drops by about 26% from a value of about $H_v = 1300$ to about $H_v = 1000$ over 80 μm. A larger drop in H_v ($\sim 40\%$) was measured for the 80/20 wt% coating; however, the overall trend of H_v as across the coating thickness is similar for both coatings.

The change in hardness may be due to the changes in the splat-cooling rates during deposition. The initial layers deposited onto the substrate undergo a more rapid cooling rate than the subsequent layers. This is caused by the ever-increasing thermal inertia of the coating during the deposition process. As the coating thickness increases, the cooling rate decreases, which may affect the microstructural evolution, such as, grain growth rates, pore production. Plasma spraying of alumina/zirconia premixed powders resulted in ceramic-composite coatings, through the thickness of functionally gradient H_v values.

3.3. X-ray analysis

Results of the X-ray analysis of the micro-composite coatings produced at high power (21.5 kW) are shown in Fig. 5. The analysis of both the 50 wt% and the 80 wt% ZrO_2/Al_2O_3 premixed powder coatings shows very similar peaks for ZrO_2 and Al_2O_3. In both cases, the much smaller Al_2O_3 peak counts indicate a significant loss of Al_2O_3 relative to ZrO_2. The melting and the boiling temperature of zirconia are about 800°C and 400°C higher than that of alumina, respectively. Thus, given similar powder properties and operating conditions, more alumina will be dissociated compared with zirconia.

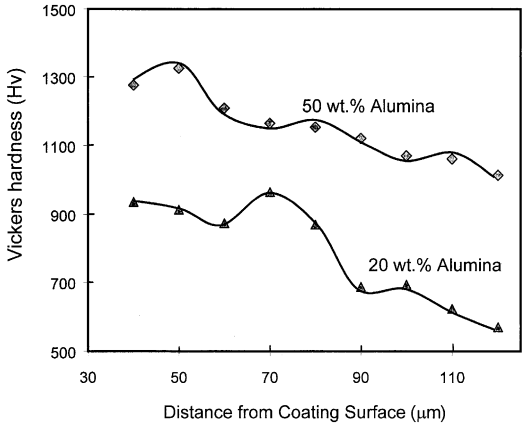

Fig. 4. Vickers hardness of the micro-composite coating deposited with a 50% and a 80/20 wt% ZrO_2/Al_2O_3 powder mixture as a function of distance from the coating surface.

4. Heat transfer analysis

A 1-d heat transfer model, based on the series calculation of thermal resistances was used by An et al. [8] and by Ravichandran [10] to evaluate the thermal conductivity of alternating YSZ–alumina coatings. The model results compared well with the measured values of thermal conductivities. We have also developed a 1-d heat transfer model, which is applicable to the composite coatings consisting of mixed YSZ and alumina splats. To accurately apply the model, detailed interface heat transfer coefficients between YSZ splats and alumina splats have to be known. Then, a range of interface coefficients to estimate the upper and lower bounds of thermal resistance of the YSZ–alumina micro-composite coatings was used.

4.1. The model

The 1-d heat transfer model is based on the series addition of thermal contact resistances comprising the thermal resistance circuit [15]. Because of the small thickness-to-width ratio of the coating, the 1-d heat transfer model is adequate to represent the thermal behavior of the coating. Fig. 6 shows the schematic of the thermal resistance circuit and the associated unit cell. The following assumptions were made for the heat transfer model:

1. Heat transfer is only perpendicular to the coating.

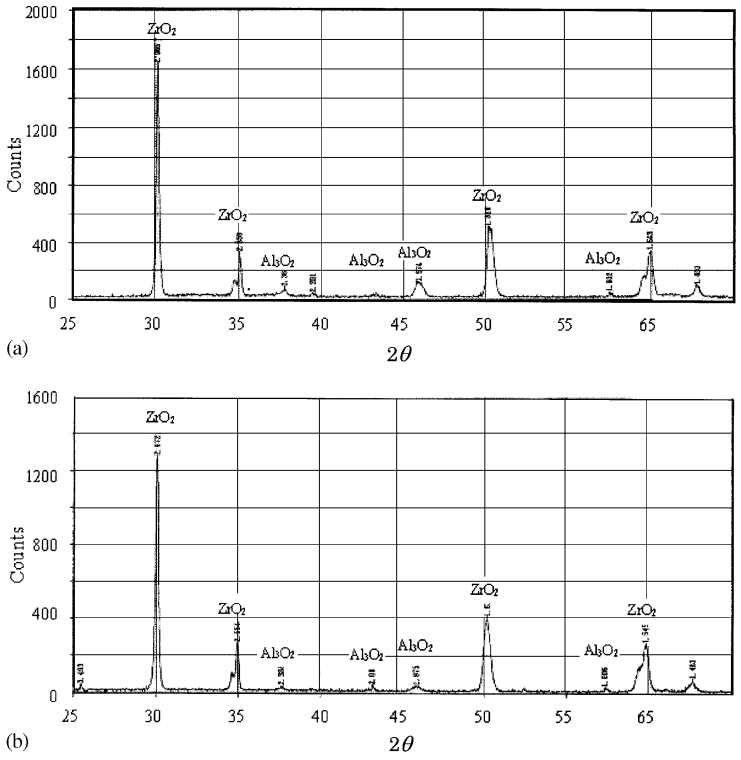

Fig. 5. X-ray diffraction patterns of micro-composite coatings. (a) 50 wt% Al_2O_3/ZrO_2, and (b) 20/80 wt% Al_2O_3/ZrO_2.

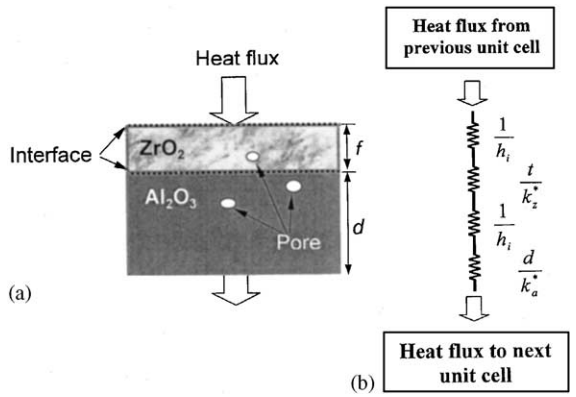

Fig. 6. Schematic of the 1-d heat transfer model. (a) The micro-composite coating unit cell, and (b) the associated thermal resistance circuit.

2. The first phase material is considered a continuous matrix, while the second phase consists of embedded splats.
3. The thickness of the embedded splats is uniform, but varies with powder weight ratio. Based on experimental observations (see Fig. 2), the minimum splat thickness is 1 μm.
4. The geometry of the embedded spats is assumed to be flat and the width of a splat determines the width of a unit cell.
5. Pores are uniformly distributed inside both phases. The interfaces between the two phases are considered free of pores.

Experimental results were used to determine several key model parameters: the minimum thickness (t) of the splats is 1 μm; the porosity is based on the image analysis of the coating and was found to be 18%; the thermal conductivity of the two phases is adjusted with this porosity; and the number of unit cells (N) through the coating is determined by $N = L/(d + t)$, where L is the coating thickness and d is the thickness of the matrix material per unit cell.

The thermal resistance (R) of the ceramic-composite zirconia–alumina coating can be defined as

$$\sum R = N\left(\frac{1}{h_i} + \frac{t}{k^{\text{eff}}_{\text{Z,A}}} + \frac{1}{h_i} + \frac{d}{k^{\text{eff}}_{\text{Z,A}}}\right), \quad (1)$$

where h_i is the interface heat transfer coefficient between zirconia and alumina splats, and $k^{\text{eff}}_{\text{Z,A}}$ are the effective thermal conductivities of zirconia or alumina corrected for porosity.

4.2. Effective thermal conductivity

Regarding the models for the effective thermal conductivity of two phase materials [16–17], the semi-empirical formula of Aiwazov and Domanshnev [18] was found to be valid for alumina having high porosities ranging form 0 to 50%. Aiwazov's formula for the effective thermal conductivity of plasma-sprayed coatings is given by

$$k_{\text{eff}}/k_{\text{m}} = (1 - P)/(1 + nP)^2, \quad (2)$$

where k_{eff} is the overall coating thermal conductivity, k_{m} is the bulk matrix material conductivity, P is the porosity, and n is an empirical constant (8, 4, 10, and 18 for alumina, zirconia, polycrystalline graphite, and silicon nitride, respectively).

Using Eq. (2), the thermal conductivity of plasma-sprayed alumina containing 18% porosity is estimated to be 3.3 W/m K (24 W/m K for k of bulk Al_2O_3). This estimate is within the range of thermal conductivity measurement values of 3–7 W/m K for Atmospheric Plasma Spray (APS) alumina between 1300 and 2100 K [19]. An average thermal conductivity value of 5 W/m K was used in our model.

Applying the Aiwazov model to zirconia coatings with a porosity of 18% results in a thermal conductivity of 0.61 W/m K, based on a bulk YSZ k value of 2.2 W/m K. Measured thermal conductivity values for 8YSZ were reported to be between 1.1 and 0.6 W/m K [20]. More recently, the thermal conductivity of plasma-sprayed 8YSZ were found to be 0.62 W/m K between 400 and 800 K [21]. So 0.62 W/m K was used as the effective thermal conductivity of 8YSZ in our model.

4.3. Splat-to-splat heat transfer coefficient

The ceramic-to-ceramic heat transfer coefficient h_i of bulk ceramics in contact with each other is reported to range between 500 and 3000 $\text{W/m}^2\text{K}$ [22]. These values are, however, not reflective of the alumina–YSZ splat-interface values, because the plasma-spray process results in the "fusion" of the two materials. The interface heat transfer coefficient of plasma-sprayed zirconia and alumina was reported and the measured heat transfer coefficients for zirconia–zirconia and alumina–alumina splat were $10^8\ \text{W/m}^2\text{K}$ at 300°C and $10^6\ \text{W/m}^2\text{K}$ at 75°C [23]. Therefore the interface heat transfer coefficient between fused alumina and YSZ phases was estimated to be of the order of 10^5–$10^6\ \text{W/m}^2\text{K}$.

4.4. Number of unit cells in the coating

To estimate the number of unit cells (N) across the coating we used the experimental observations for the 80/20 and 50 wt% composite coatings (Fig. 2). For premixed powder sizes between 10 and 53 μm diameter, the minimum splat thickness was 1 μm. The unit-cell is defined as containing at least 2 phases as shown schematically in Fig. 6. The number of unit cells across the coating for the 80/20 and 50 wt% powder mix is estimated to be about 5 and 25, respectively. The thickness of each phase per unit cell was determined as a function of powder weight ratio. Fig. 7 shows the number of unit cells and the splat thickness of each phase associated with a unit cell as a function of powder mixture ratio.

4.5. Heat-transfer model results

The results of the series-calculated thermal resistance is plotted as a function of powder-mixture weight ratio in Fig. 8. For h_i between 3000 and $310^5\ \text{W/m}^2\text{K}$, the analysis shows that the addition of <50 wt% of alumina decreases the overall thermal conductivity of the composite YSZ–alumina coatings. The alumina can serve as a second phase material, which increases the resistance to thermal shock and reduces oxygen diffusion through YSZ-based coatings without

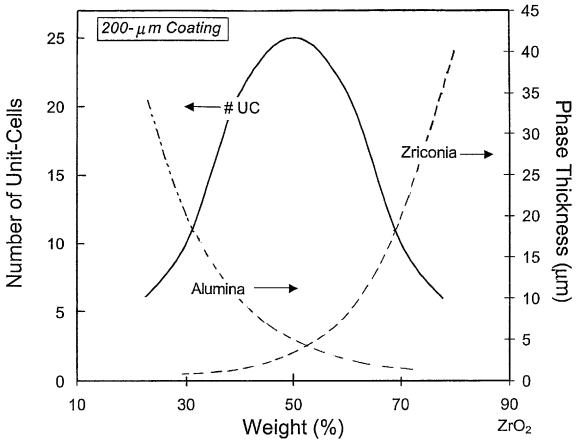

Fig. 7. Number of unit cells across a 200 μm thick coating and the associated thickness of the constituent phases per unit cell as a function of powder mixture wt%.

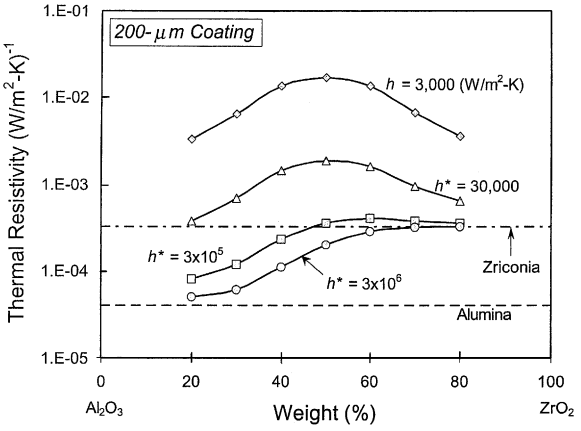

Fig. 8. Thermal resistance of 200 μm thick micro-composite coatings for alumina–zirconia interface heat transfer coefficients between 3000 and $3 \times 10^6\,\mathrm{W/(m^2\,K)}$ as a function of powder mixture wt% (cf.: the resistances of 18% porous YSZ and alumina coatings).

compromising the thermal behavior of YSZ-based TBCs.

Fig. 9 shows the series calculated thermal conductivity of the micro-composite coating in comparison with bulk alumina and bulk and plasma-sprayed 8YSZ. The 8YSZ thermal conductivity is relatively independent of temperature, while that of the bulk alumina is not. The temperature dependence of effective thermal conductivity of the micro-composite coatings was

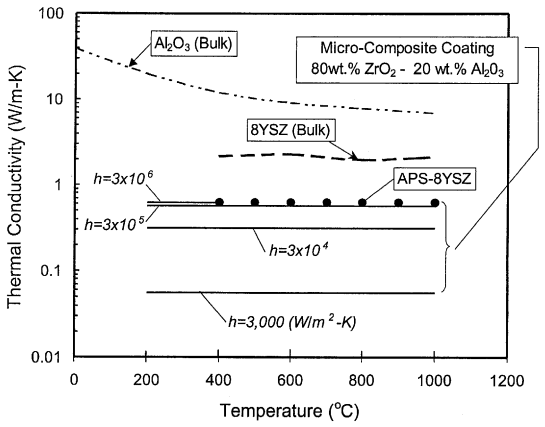

Fig. 9. Thermal conductivity of bulk alumina 8-YSZ and estimated range of thermal conductivity of a micro-composite coating containing 18% porosity and made with a premixed powder of 8-YSZ and 20 wt% Al_2O_3.

evaluated for a 20 wt% alumina mixture and is shown in Fig. 9. It can be seen that k_{eff} of the composite is independent of temperature and that it drops sharply for h_i values smaller than $310^4\,\mathrm{W/m^2\,K}$. A significant drop in thermal conductivity was measured in plasma-sprayed alternating alumina–zirconia coatings [9,10].

A reasonable h_i value for alumina/zirconia interfaces will thus lie between 3×10^4 and $3 \times 10^5\,\mathrm{W/m^2\,K}$. Therefore, based on our heat transfer model, coatings produced with as little as 20 wt% alumina can exhibit an increase in thermal resistance by as much as a factor of two, relative to pure YSZ-based coatings.

Thus, micro-composite YSZ-based TBCs can be produced with alumina as a second phase material. Inclusion of alumina can result in improved mechanical and chemical properties, such as, decrease in residual stress and oxygen diffusion.

5. Conclusions

Using mixtures of 8YSZ and Al_2O_3 powder, micro-composite coatings were plasma-sprayed onto stainless steel coupons with the gas tunnel-type plasma spraying. The coatings exhibited a ceramic composite morphology consisting of

splats of the lesser constituent imbedded in the host ceramic matrix. The ceramic composites exhibited the following physical characteristics:

(1) The splat geometry depends on the powder mixing ratio between the ZrO_2 and Al_2O_3 phases: at higher alumina content, the imbedded splats become "flatter" and more parallel to the substrate.
(2) Plasma spraying of premixed alumina and zirconia powders results in a reduction of porosity, compared with coatings produced with 100% of either constituents. The micro-composite constituent ratio is not only a function of the starting powder mixture ratio, but also depends on the operating power: high-power operation results in relatively more loss of alumina compared with zirconia.
(3) The coating hardness increased with an increase in alumina content. The variation of H_v with spraying distance was independent of powder mixture: both the 50 and 20 wt% powder mixtures exhibit similar H_v -to-spraying distance behavior.
(4) Hardness measurements across the micro-composite coating show an increase in hardness towards the coating surface, which indicates a coating with a functionally gradient hardness.

A 1-d heat transfer model was developed, which takes into account the effects of splat topology as a function of powder mixing ratio. The model predicted the effects of varying powder mixtures on the overall thermal resistance of the composite coatings.

(1) The thermal resistance of the micro-composite coating spans the range between pure alumina and pure YSZ. For premixed powders containing <20 wt% alumina, the model predicted an increase in the overall thermal resistance of the composite coating by as much as a factor of two.
(2) A heat transfer coefficient range between 3000 and $3\times10^6\,W/m^2\,K$ was used based on the published ceramic-to-ceramic and splat-to-splat data.
(3) Micro-composite TBCs can be plasma-sprayed with improved mechanical and chemical properties without compromising the thermal behavior of the coatings.

Acknowledgements

The authors thank the Ministry of Education (Monbusho, Japan) and the Joining and Welding Research Institute, Osaka University (Japan) for partial support of this project.

References

[1] Berndt CC. Proceedings of the First United Thermal Spray Conference. Materials Park, OH: ASM International, 1998.
[2] Yonushonis TM. Therm J Spray Technol 1997;6(1):50–6.
[3] Brindley WJ, et al. Proceedings of a Conference held at and Sponsored by NASA Lewis Research Center, National Aeronautics and Space Administration, Office of Management, Scientific and Technical Information Program, 1995.
[4] Narendra BD, Janet MH, Jacob J. Stiglich, Proceedings of a Symposium, High Temperature Coatings—I. Warrendale, PA: Minerals, Metals & Materials Society, 1995.
[5] Heimann RB. Plasma-spray coating. New York, NY, USA: VCH Publishers, Inc., 1996.
[6] Steffens HD, Babiak Z, Gramlich M. Therm J Spray Technol 1999;8(4):517–22.
[7] Srivatsan TS, et al. Proceedings of the 1997 ASME International Mechanical Engineering Congress and Exposition. New York, NY: American Society of Mechanical Engineers, 1997.
[8] An K, Ravichandran KS, Dutton RE, Semiatin SL. J Am Ceram Soc 1999;82(2):399–406.
[9] Ramaswamy P, Seetharamu S, Varma KBR, Rao KJ. Comput Sci Technol 1997;57:81–9.
[10] Ravichandran KS, An K, Dutton RE, Semiatin SL. J Am Ceram Soc 1999;82(3):673–82.
[11] Green DJ, Cai PZ, Messing GL. J Eur Ceram Soc 1999;19:2511–7.
[12] Kobayashi A. Mater Eng Performance 1996;5:373.
[13] Scion Image, Version 4, Scion Corp. Maryland 21701, USA.
[14] Doerner P, et al. CALPHAD: Comput Coupling Phase Diag Thermochem 1979;3(4):241–57.
[15] Mills AF. Basic heat and mass transfer, 2nd ed. Englewood Cliffs, NJ: Prentice Hall, 1999.
[16] Maxwell JC. Atreatiseonelectiricty, magnetism, 3rd ed. New York: Dover, 1954. p. 1 [Chapter 9].

[17] Bruggeman D. Ann Phys 1935;24:636.
[18] Aiwazow MI, Domashnev IA. Proshk Metall 1968;8:51.
[19] Wilkes KE, Lagedrost JF. NASA Rep. CR-121144, March 1073.
[20] Pawlowski L, Lombard D, Fauchais P. J Vac Sci Technol 1985;A3(6):2494–500.
[21] Slifkaa AJ, Fillaa BJ, Phelpsa JM, Banckeb G, Berndtb CC. J Therm Spray Technol 1998;7(1):43–6.
[22] Raznjevic K. Handbook of thermodynamic tables and charts. New York: McGraw-Hill, 1976.
[23] Bianchi L, Denoirjean A, Blein F, Fauchais P. Thin Solid Films 1997;299:125–35.